NUCL SCI TECH (2021) 32:123
https://doi.org/10.1007/s41365-021-00968-x

Neutronics analysis of a stacked structure for a subcritical system with LEU solution driven by a D-T neutron source for ^{99}Mo production

Lei Ren[1,2] · Yun-Cheng Han[1] · Jia-Chen Zhang[1,2] · Xiao-Yu Wang[1,2] · Tao-Sheng Li[1] · Jie Yu[1]

Received: 24 May 2021 / Revised: 16 September 2021 / Accepted: 19 September 2021 / Published online: 16 November 2021

Abstract The utilization of neutrons markedly affects the medical isotope yield of a subcritical system driven by an external D-T neutron source. The general methods to improve the utilization of neutrons include moderating, multiplying, and reflecting neutrons, which ignores the use of neutrons that backscatter to the source direction. In this study, a stacked structure was formed by assembling the multiplier and the low-enriched uranium solution to enable the full use of neutrons that backscatter to the source direction and further improve the utilization of neutrons. A model based on SuperMC was used to evaluate the neutronics and safety behavior of the subcritical system, such as the neutron effective multiplication factor, neutron energy spectrum, medical isotope yield, and heat deposition. Based on the calculation results, when the intensity of the neutron source was 5×10^{13} n/s, the optimized design with a stacked structure could increase the yield of ^{99}Mo to 182 Ci/day, which is approximately 16% higher than that obtained with a single-layer structure. The inlet H_2O coolant velocity of 1.0 m/s and initial temperature of 20 °C were also found to be sufficient to prevent boiling of the fuel solution.

This work was supported by the Natural Science Foundation of Anhui Province (No. 1808085MA10), Anhui Provincial Key R&D Program (No. 202104g0102007), and the National Natural Science Foundation of China (No. 21805283).

✉ Yun-Cheng Han
yuncheng_han@163.com

1 Hefei Institutes of Physical Science, Chinese Academy of Sciences, Hefei 230031, China

2 University of Science and Technology of China, Hefei 230026, China

Keywords Neutronics analysis · Stacked structure · ^{99}Mo yield · Subcritical system · D-T neutron source

1 Introduction

^{99m}Tc is currently the most commonly used medical radionuclide for diagnosis and treatment owing to its excellent nuclear imaging properties [1]. For example, a half-life of approximately 6 h indicates that ^{99m}Tc can enable rapid imaging after entering the human body, and the emitted gamma rays with an energy of 141 keV can penetrate most tissues and organs of humans without obvious harm [2]. The medical use of ^{99m}Tc is mainly derived from ^{99}Mo decay with a half-life of approximately 66 h, which is predominantly produced by two traditional methods via the fission reaction of ^{235}U(n, f) ^{99}Mo, and the activation reaction of ^{98}Mo(n, γ) ^{99}Mo, as shown in Fig. 1 [3, 4]. Compared with the activation method, the use of the fission method to produce ^{99}Mo is associated with advantages such as higher yield, higher specific activity, and lower cost [5]. Currently, the fission method accounts for approximately 75% of the world's ^{99}Mo production owing to the irradiation of highly enriched uranium (HEU) targets in six experimental reactors, such as the National Research Universal reactor in Canada, the Belgian Reactor-2 in Belgium, and the High Flux Reactor in the Netherlands [6]. Most of these reactors are aging, with an average operating life of over 40 years; accordingly, they are facing the problem of retirement [7]. In recent years, unscheduled reactor shutdowns have frequently occurred for technical maintenance and repair [8]. However, the elimination of HEU target irradiation is increasingly being advocated to avoid the threat of nuclear proliferation [9]. In general, the

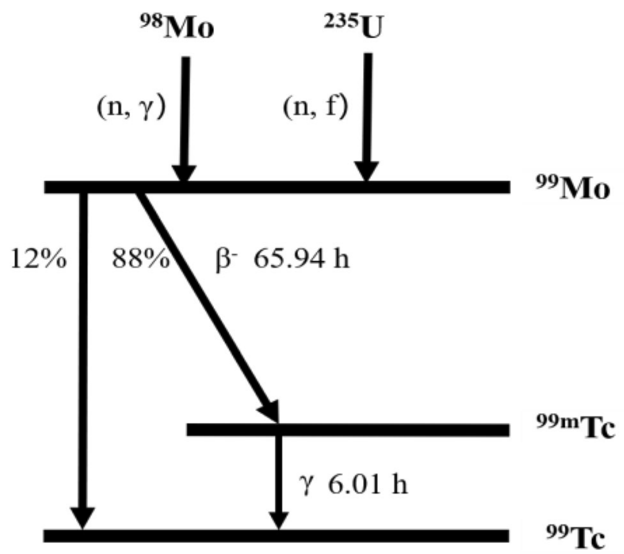

Fig. 1 Two traditional methods of producing ^{99}Mo and the decay scheme of ^{99}Mo/^{99m}Tc

prohibition of HEU and frequent reactor shutdown accidents have caused a serious crisis in the global supply of ^{99}Mo, leading to the delay or cancelation of many medical procedures [10].

Several new methods have been proposed to produce ^{99}Mo in a safer, cleaner, more affordable, and capable manner. These methods can be divided into three categories: (1) accelerator-based production methods, including ^{98}Mo(n, γ) ^{99}Mo, ^{238}U(γ, f) ^{99}Mo, and ^{100}Mo(γ, n) ^{99}Mo; (2) solution reactor-based methods, such as the use of the medical isotope production reactor (MIPR) and molten salt reactor (MSR); and (3) methods based on a combination of the accelerator and solution fuel, such as the use of a subcritical system driven by an external neutron source [11–17]. The third method has become one of the best choices for ^{99}Mo production owing to the following advantages: (1) the solution target can be recycled efficiently, which markedly reduces the generation of radioactive waste, compared with that of accelerator-based production methods that use solid targets; (2) the third method is markedly safer than MIPR as the use of an external accelerator-based neutron source to drive the subcritical system avoids the generation of criticality accidents; and (3) building new subcritical systems is associated with a shorter approval cycle and lower approval difficulty than MIPR [18–21]. However, the neutron flux of an accelerated-based D-T neutron source is markedly lower than that of the experimental reactor, and the efficient use of source neutrons is the key issue for the application of this new production method. In 2011, a subcritical system with LEU solution driven by an external D-T neutron source was proposed to produce at least one-half of the U.S. demand for ^{99}Mo by SHINE Medical Technologies, which increased the utilization of the D-T neutron source by adding functional components of a neutron multiplier and a neutron reflector. The calculation results revealed that the neutron multiplier increased the level of thermal neutron flux by moderating and multiplying neutrons, and the neutron reflector could effectively reduce neutron leakage by 80–90% [22, 23]. The subcritical assembly for ^{99}Mo production (SAMOP) is similar to the SHINE design principle, which increased the utilization of neutrons by applying similar methods [24]. Pardo's team from Cuba used a D-T neutron source and an ARGUS reactor model containing LEU solution for isotope production, which increased the utilization of neutrons owing to the use of a neutron moderator and a neutron reflector [25]. Y. Han's team from China explored the influence of geometrical dimensions, such as the neutron multiplier and the neutron reflector, on the neutronics performance of the subcritical system to optimize the geometric dimensions. As a result, they obtained an ^{99}Mo yield of 167 Ci/day [26]. According to previous research, the utilization of source neutrons can be effectively improved by using a moderator to regulate the neutrons, a multiplier to increase the neutrons, a reflector to reduce neutron leakage, as well as optimization of the geometric dimensions. The structure of the above-mentioned subcritical system is basically a single-layer structure consisting of an external neutron source, multiplier, LEU solution, reflector, and shield from inside to outside, which does not fully utilize neutrons that backscatter to the source direction. The stacked structure is formed by the neutron multipliers and LEU solution layers being multi-layer (layers $\geq$ 2) and arranged across each other, as shown in Fig. 2, which can enable better use of the neutrons scattered in the source direction. The number of neutron multipliers and LEU solution layers is referred to as the number of stacked pairs.

The utilization efficiency of source neutrons was improved in this study by introducing a stacked structure. The objective of this study was to determine the effect of the number of stacked pairs on the reactivity of a subcritical system and to evaluate the neutronics and safety behavior of the system in steady-state operation. Neutronic and safety studies have sought to evaluate parameters, such as neutron effective multiplication factor, thermal power, neutron flux density distribution, and yields of medical isotopes.

2 Model and methods

2.1 Description of the subcritical system

The subcritical system with a stacked structure is roughly a nested concentric cylinder with a gas target

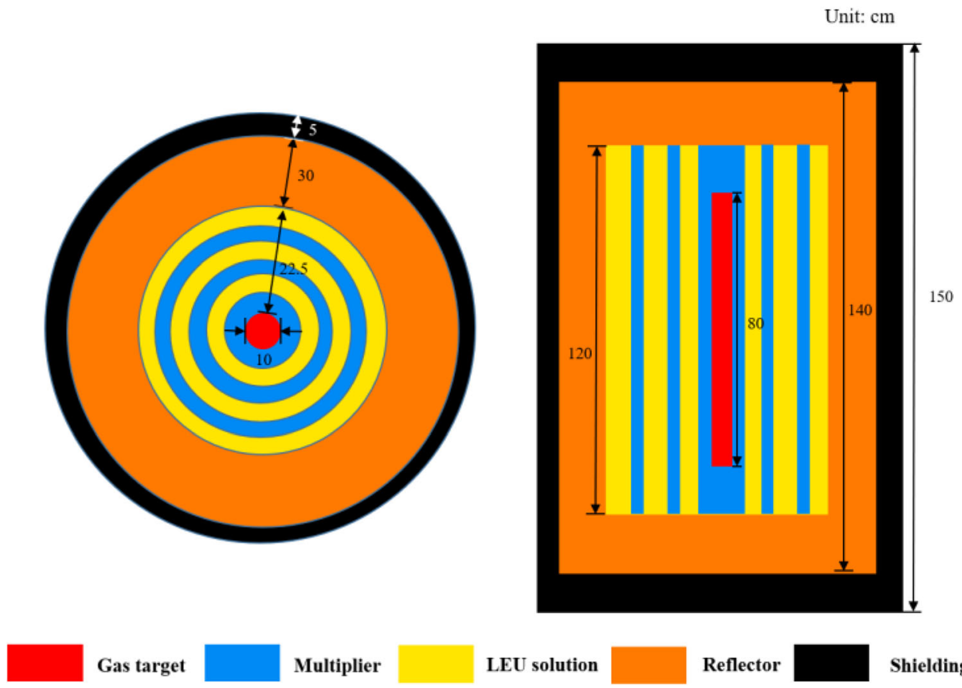

Fig. 2 (Color online) Basic scheme of the stacked subcritical system without cooling and containers

chamber in the middle, as shown in Fig. 2, and a stacked structure composed of multipliers and LEU solution, a reflector, and a shield outward. The dimensions of the subcritical system, as shown in Fig. 2, were fixed according to the preliminary analysis results. A similar subcritical system with a single-layer structure has been described in detail elsewhere [26]. The D^+ ion beam is accelerated by the linear accelerator into the T_2 gas target cavity located in the middle of the subcritical system and induces the D-T fusion reaction to produce primary neutrons. After the multiplier's multiplication and moderation adjustment, neutrons enter the LEU solution to induce ^{235}U fission and generate ^{99}Mo. After irradiation with neutrons, the LEU solution enters the separation and purification unit for ^{99}Mo extraction and separation, and the final medicine is delivered to the hospital as an $^{99}Mo/^{99m}Tc$ generator for treatment. The separation LEU solution re-enters the reaction zone after concentration and acidity adjustment, and receives irradiation in the next cycle. The cooling system is composed of a coiled cooling pipe, which ensures that the working temperature of the LEU solution is below 90 °C.

2.2 The accelerator-based D-T fusion neutron source

The accelerator-based D-T fusion neutron source is critical for subcritical systems. The high-intensity D-T fusion neutron generator (HINEG), developed by the Chinese Academy of Sciences, has a neutron source strength of 6.4×10^{12} n/s, which will provide the experimental research basis for this study. The working principle of the D-T fusion neutron source is as follows: the radio frequency antenna is used to strip the deuterium atoms to form a deuterium ion beam, which is focused by the director, and the four-stage lens to bombard the gaseous tritium target to produce a strong current of neutrons. HINEG's technical upgrade will help to achieve the target parameters of this study [21, 27]. The key properties of the neutron source used in this study are listed in Table 1.

2.3 Materials

The following materials were selected for use in the subcritical system: (I) Be was selected as the multiplier, which is consistent with previous research, to further increase the neutron flux and the uranium utilization rate in the LEU solution zone. The Be material also moderates the neutrons; (II) the Zr-4 alloy, SS304 stainless steel, and 6061-Al alloy were selected as candidate container materials to hold the LEU solution. These materials are commonly applied in pressurized water reactors as fuel containers and core structural materials owing to their good corrosion resistance, suitable mechanical properties, and

Table 1 Key properties of the required neutron source

Physics parameters	Value
Total intensity of the neutron source	5×10^{13} n/s
Energy of the primary neutron	14.1 MeV

low thermal neutron absorption cross-section [28, 29]; (III) the UO_2SO_4 solution was selected as the fission fuel owing to its good radiation stability. The uranium concentration was 75 g/L and the enrichment of ^{235}U was 19.75%; (IV) light water (H_2O) was selected as the coolant for the subcritical system; (V) graphite was used to form the reflector, which is used to surround the LEU solution zone, as employed in previous studies; (VI) SS304 boron steel was selected as the shielding material owing to its excellent nuclear shielding performance and good mechanical properties. The steel can also be used as the structural material to support the system. In the final design, the concrete material was further added outside the SS304 boron steel shield to achieve a double-layer shielding structure. The main specifications of the subcritical system are listed in [30] Table 2.

2.4 Calculation method

2.4.1 Program

Neutron calculations of the subcritical system were carried out using the Super Monte Carlo Simulation Program for Nuclear and Radiation Process (SuperMC) version 3.2, which was coupled with the hybrid evaluation nuclear data library system [31]. Herein, the steady-state neutronics parameters of the subcritical system mainly included the neutron effective multiplication factor, neutron energy spectrum, medical isotope yield, and heat deposition. Thermal analysis of the subcritical system was performed using COMSOL software to design the cooling system, which has sufficient cooling performance to prevent boiling of the fuel solution [8].

2.4.2 Uncertainty

Generally, one calculation requires a random process of hundreds of thousands of particles to satisfy the statistical reliability, tracking each particle from the source to being absorbed or escaping, and recording its reaction in real-time. In this study, the number of statistical particles was 10 million in each neutronics calculation, and the corresponding statistical uncertainties did not exceed 1%. Except for the calculations of energy deposition and neutron flux density distribution, the statistical uncertainties were less than 3%.

2.4.3 Definition and equation

Criticality calculation: Estimating the safety of a subcritical system by the effective subcritical neutron multiplication factor with external neutron source k_s is conservative and feasible, as k_s is greater than the effective neutron multiplication factor k_{eff} in the presence of an external neutron source inside the nuclear fuel. The state of criticality can be concisely summarized by k_s, which is defined as the ratio of fission neutrons to the total number of neutrons (i.e., fission neutrons and external neutron source) in the system [32]:

$$\frac{1}{k_s} = 1 + \frac{S_0}{\nu W}, \tag{1}$$

where S_0 is the intensity of the neutron source [n/s], ν is the average number of neutrons generated in a fission reaction, and W is the fission reaction rate [fissions/s].

The utilization rate of uranium was evaluated according to the definition of specific activity (*SA*) [Ci/kg], which is obtained by the yield of ^{99}Mo per unit mass of ^{235}U in the

Table 2 Material parameters of each area of the subcritical system

Zone	Materials	Element mass ratio (W%)	Density (g/cm^3)
Target	Tritium (gas)	^{3}H:100.00	2.70×10^{-6}
Multiplier	Beryllium	^{9}Be:100.00	1.85
Fuel solution	75 g·U/L UO_2SO_4	^{235}U:1.37, ^{238}U:5.57, ^{16}O:82.20, ^{32}S:0.94, ^{1}H:9.92	1.08
Container 1	Zr-4 alloy	^{94}Zr:98.20, ^{88}Sr: 1.50, ^{56}Fe:0.20, ^{52}Cr:0.10	6.55
Container 2	SS304 stainless steel	^{56}Fe:69.50, ^{52}Cr:19.00, ^{58}Ni:9.50, ^{55}Mn:2.00	7.93
Container 3	6061-Al alloy	^{27}Al:97.85, ^{56}Fe:0.50, ^{58}Ni:0.60, ^{48}Ti:0.15, ^{52}Cr:0.20, ^{65}Zn:0.25, ^{24} Mg:0.10, ^{55}Mn:0.15, ^{63}Cu:0.20	2.75
Coolant	Light water	^{1}H:11.11, ^{16}O:88.89	1.00
Reflector	Graphite	^{12}C:100.00	1.70
Shield	SS304 boron steel	^{56}Fe:67.42, ^{52}Cr:19.00, ^{58}Ni:9.50, ^{55}Mn:2.00, ^{28}Si:1.00, ^{12}C:0.08, ^{32}S:0.03, ^{31}P:0.045, ^{10}B:1.00	7.93

uranium solution with irradiation for 1 day. The calculation method is as follows:

$$SA = \frac{A}{m} = \frac{\lambda N}{m} = \lambda RTS_0 \frac{N_A}{M} \times \eta_{Mo-99}, \tag{2}$$

where η_{Mo-99} is the fission branch ratio of ^{99}Mo, and the value for ^{235}U fission is 6.1%, which can be found at (www-nds.iaea.org/sgnucdat/c3.htm#92-U-235), A is the total yield of ^{99}Mo [Ci], N is the number of generated ^{99}Mo [atoms], m is the mass of ^{235}U [g], T is the irradiation time period [s], M is the relative atomic mass of ^{235}U, N_A is the Avogadro constant (6.02×10^{23}), and λ is the decay constant of ^{99}Mo (0.0105 h^{-1}).

Burnup calculation: The goal is to obtain the changes in fuel components over time; its main task is to solve the following equations [33]:

$$\frac{dN_i}{dt} = -(\lambda_i + \sigma_i \varphi)N_i + \sum_{j \neq 1} N_j(\lambda_{ij} + \sigma_{ij}\varphi) + S_i, \tag{3}$$

$$S_i = \sum_k N_k \sigma_k^f \varnothing Y_{ik}, \tag{4}$$

where N_i represents the nuclear density of nuclide i at time t [$\times 10^{24}$ cm^{-3}]; λ_i and λ_{ij} represent the decay constant of nuclide i and the decay constant of nuclide j to i [s^{-1}]; σ_i, σ_{ij}, and $\sigma_k^{\,f}$ represent the total reaction cross-section of nuclide i, the reaction cross-section of nuclide j to nuclide i, and the fission cross-section of nuclide k [b]; S_i is the source of the fission reaction to produce nuclide i; and Y_{ik} represents the share of fission products from nuclide k to nuclide i.

Void coefficient calculation: The water in the LEU solution undergoes radiolysis to generate H_2 and O_2 during the irradiation process. These gases form bubbles in the solution and continue to rise to the surface of the solution, causing the LEU solution to “boil,” which has an obvious impact on the reactivity of the system. The void coefficient α_V is defined as the reactivity change caused by a 1% change in the volume fraction of the cavity in the LEU solution:

$$\alpha_V = \frac{d\rho}{d\alpha} = \frac{1}{k}\frac{dk}{d\alpha}, \tag{5}$$

where α is the void fraction, ρ is the reactivity of the system, and k is the effective multiplication coefficient of neutrons.

The calculation methods for other parameters, such as the neutron flux density distribution, heat deposition, and reaction rate, follow similar methods described elsewhere in detail [26].

3 Results and discussion

3.1 Influence of the number of stacked pairs on the subcritical system

3.1.1 Keeping the total width of the multiplier and fuel solution constant

In this section, the impact of the stack structure on the system under ideal conditions, which do not consider the cooling system and fuel containers, is discussed. The change in the LEU solution volume with the number of stacked pairs when the total width of the multiplier and fuel solution are kept constant, is shown in Fig. 3a. The volume of the LEU solution was found to sharply decrease and then gradually saturate as the number of stacked pairs approached eight. This is because the multiplier occupies more volume with an increase in the number of stacked pairs. The ^{99}Mo yield and ^{99}Mo yield per unit volume varying with the number of stacked pairs are shown in Fig. 3b. The trend of the ^{99}Mo yield with the number of stacked pairs was observed to be roughly the same as the volume of the LEU solution. The ^{99}Mo yield per unit volume increased with the increase in the number of stacked pairs until saturation, with the maximum reaching 0.94 Ci/L. Such a finding indicates that the stacked structure can improve the reactivity of the system because the yield of ^{99}Mo per unit volume changes completely, opposing the yield of ^{99}Mo.

3.1.2 Keeping the total volumes of the multiplier and fuel solution constant

In this section, the impact of the stacked structure on the system under ideal conditions, while the total volumes of the multiplier and the fuel solution are kept constant, is explored. The influence of the number of stacked pairs on the yield of ^{99}Mo is shown in Fig. 4. When the number of stacked pairs was four, the yield of ^{99}Mo reached a maximum value of 190 Ci/day, which was 17% higher than that with a single-layer structure (162 Ci/day). This finding is because the neutrons scattered in the source direction can be fully utilized when the number of stacked pairs increases in the early stage. As the number of stacked pairs continues to increase, the multipliers contribute more to neutron absorption. As a result, some neutrons cannot enter the LEU solution to induce the fission reaction, leading to a decrease in the yield of ^{99}Mo. Overall, the stacked structure can increase the reactivity of the system under ideal conditions, which is consistent with the conclusion of the previous section.

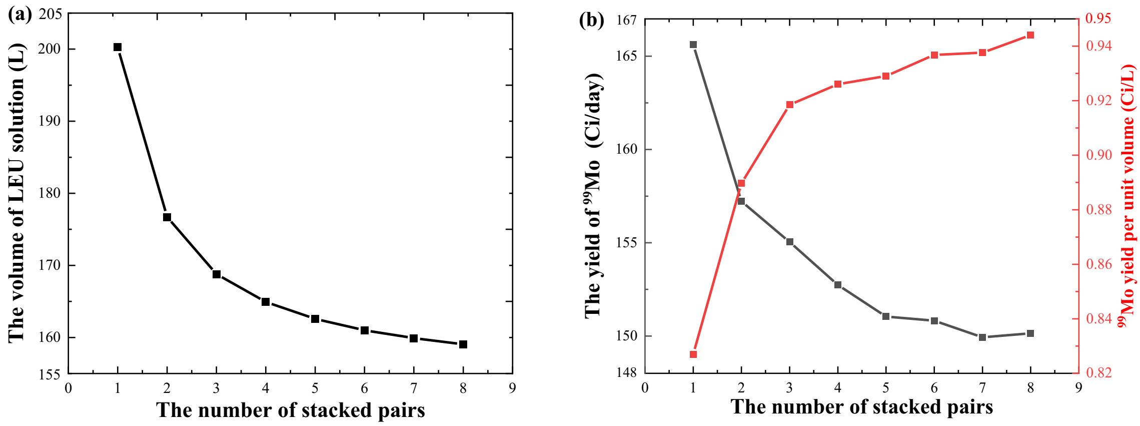

Fig. 3 **a** The LEU volume; **b** the ^{99}Mo yield and ^{99}Mo yield per unit volume varying with the number of stacked pairs when width is kept constant

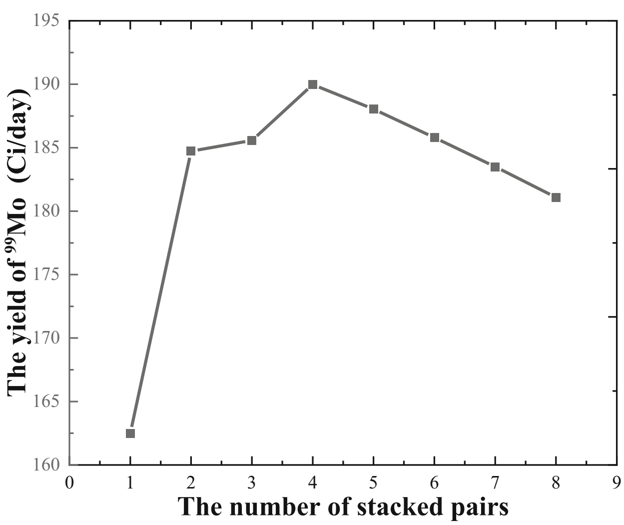

Fig. 4 ^{99}Mo yield varying with the number of stacked pairs when volumes are kept constant

3.2 Impact of the cooling system and container materials

We explored the influence of the number of stacked pairs on the system under ideal conditions in Sect. 3.1, and proved that the use of the stacked structure is beneficial for increasing the reactivity of the subcritical system. However, the cooling system and the use of fuel container materials in the actual situations need to be considered. Based on the model in Fig. 2, when the total volumes of the multiplier and fuel solution are kept constant, the yields of ^{99}Mo were calculated with the number of stacked pairs under different conditions of container materials (Zr-4 alloy, SS304 stainless steel, and 6061-Al alloy) coupled with the coolant material (H_2O), as shown in Fig. 5a. When Zr-4 alloy was employed as the container material, the highest ^{99}Mo yield was obtained relative to that achieved with the other two materials. The yield of ^{99}Mo with the Zr-4 alloy container reached the maximum when the number of stacked pairs was three, which is two for the SS304 stainless steel and 6061-Al alloy. Such finding indicates that the Zr-4 alloy has the least influence on neutrons compared to the other two materials. Therefore, the Zr-4 alloy was selected as the container owing to its good corrosion resistance, suitable mechanical properties, and low thermal neutron absorption.

The yield of ^{99}Mo first increases and then decreases with an increase in the number of stacked pairs according to the "Zr-4 alloy" curve in Fig. 5a. The overall yield of ^{99}Mo was slightly lower than that of the ideal situations in Fig. 4, which indicates that the Zr-4 alloy is not as capable of neutron multiplication as neutron absorption under this condition. When the number of stacked pairs was three, the yield of ^{99}Mo could reach a maximum of 182 Ci/day, which is almost 16% higher than that with a single-layer structure (157 Ci/day). This result is because with an increase in the number of stacked pairs, the neutrons scattered in the source direction can be fully utilized for the same reason under ideal conditions; however, as the number of stacked pairs continues to increase, the neutron absorption effect of the container material is enhanced, resulting in a faster decline in the yield of ^{99}Mo than that under ideal conditions. Based on the influence of stacked pairs on k_s, when the number of stacked pairs was three, k_s increased to the maximum value of 0.954, as shown in Fig. 5b. This increase further illustrates that the use of a stacked structure is beneficial for increasing the reactivity of the subcritical system. Based on the above calculation results, three was selected as the best number of stacked pairs.

From the definition of k_s in formula (1), the number of fission is proportional to $k_s/(1\text{-}k_s)$, and the yield of ^{99}Mo is proportional to the number of fission; thus, the yield of

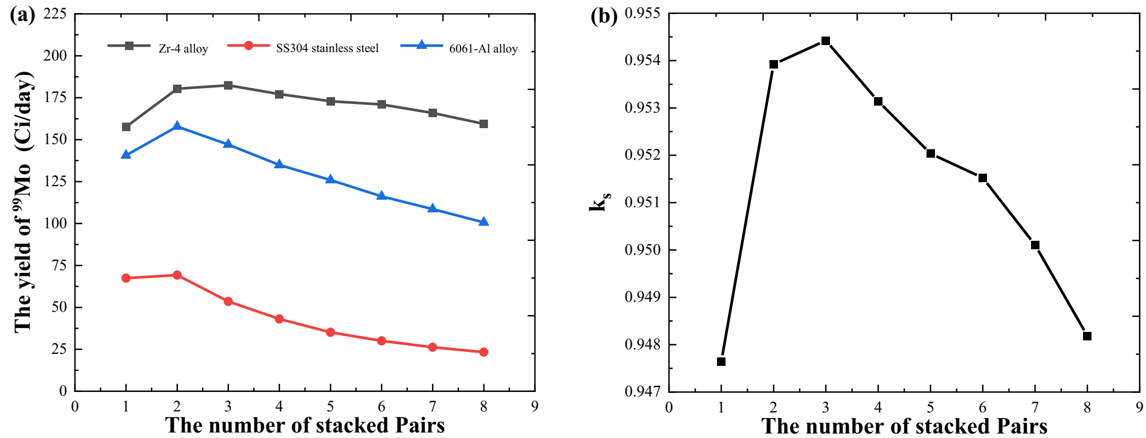

Fig. 5 **a** ^{99}Mo yields varying with container materials; **b** the k_s of Zr-4 alloy varying with the number of stacked pairs

^{99}Mo is also proportional to $k_s/(1\text{-}k_s)$. The ^{99}Mo yield varying with k_s can be obtained by combining the above calculation results, as shown in Fig. 6, whose trend is similar to that of $k_s/(1-k_s)$ varying with k_s. Therefore, despite changes in the thickness and uranium concentration, the greater the k_s, the higher the ^{99}Mo yield. The subcriticality can be further tuned to increase the yield of ^{99}Mo by increasing uranium concentration, and the corresponding cooling system must be adjusted according to the thermal power.

The evolution of k_s over ten full-power years was calculated, reaching a fuel burnup of 3542 kWd/kgU, as shown in Fig. 7. An important parameter in the operation of a nuclear system is the fissile fuel consumption and fissile isotope production, which are mainly ^{235}U and ^{239}Pu in the current study. The consumption of ^{235}U was approximately 0.094 g in the study subcritical system for a 5-day irradiation cycle, and approximately 2.2% of the

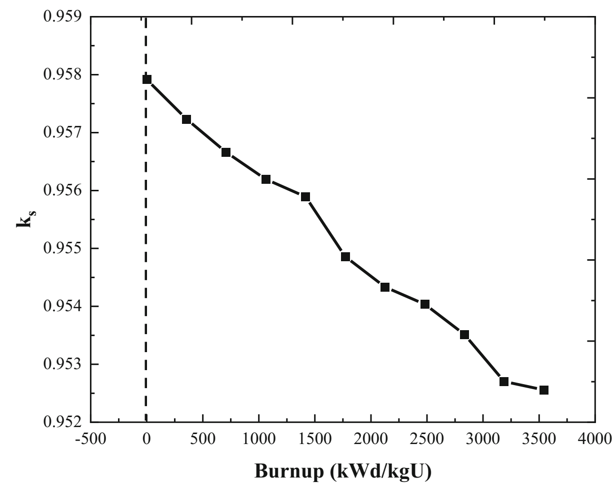

Fig. 7 k_s varying with the burnup under the condition of 3 stacked pairs

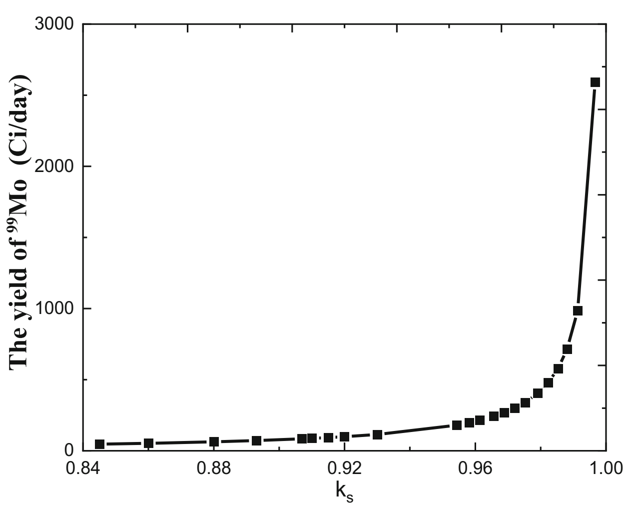

Fig. 6 ^{99}Mo yield varying with k_s under the condition of 3 stacked pairs

total content even after running 10 full power years. The results of ^{239}Pu displayed a linear growth proportional to the time of burnup, reaching only 3.788 g of ^{239}Pu at the end of a burnup cycle of 10 years. In addition, 0.022 g of ^{240}Pu and 8.967 g of ^{236}U were generated after 10 full power years. The contents of other uranium isotopes and transuranic nuclides, such as ^{234}U, ^{237}U, ^{239}Np, and ^{237}Np, were less than 1 mg.

The capability of the system to produce medical isotopes was evaluated. The accumulation of ^{99}Mo in 168 h under normal operating conditions is shown in Fig. 8a. The ^{99}Mo inventory grows exponentially and reaches saturation activity. Based on the calculations, 570 Ci and 606 Ci of ^{99}Mo were produced in 5 and 7 days, respectively. In addition, as shown in Fig. 8b, the yields of other useful medical radioisotopes, such as ^{133}Xe, ^{131}I, and ^{89}Sr, were calculated, which confirmed that the subcritical system has great potential for medical isotope production.

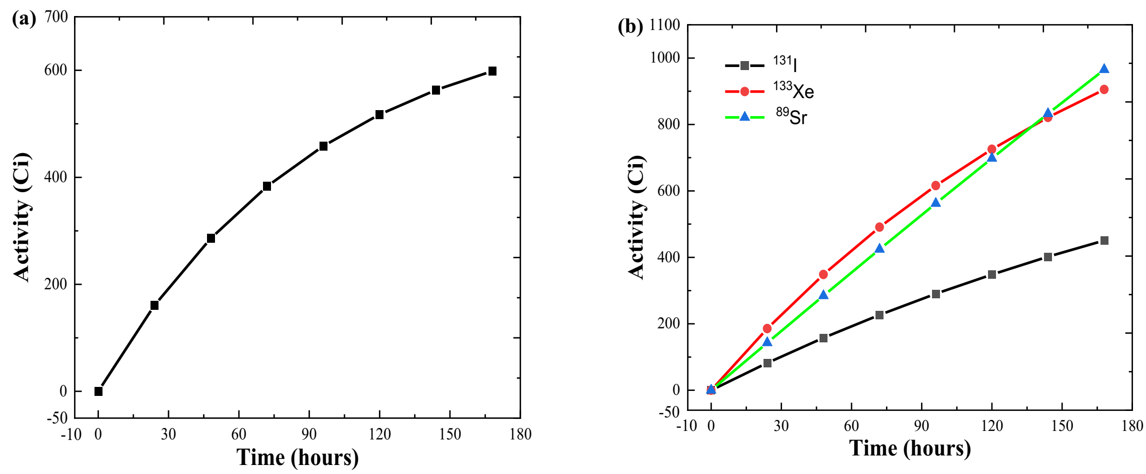

Fig. 8 Accumulation of the medical isotopes during 168 h of system operation: **a** ^{99}Mo; **b** ^{133}Xe, ^{131}I, and ^{89}Sr

3.3 Calculation of neutron flux density distribution

To more intuitively obtain the neutron flux density distribution in the LEU solution area, a grid counter card was used to calculate the entire area after cutting along the axis, including the neutron source, stacked-structure area, reflector, and shield. The neutron flux density distribution in the subcritical system is shown in Fig. 9a. As the distance from the source increased, the neutron flux density distribution was found to gradually decrease. The neutron flux density distribution in the entire subcritical system is related to the structural layout and radiates in an elliptical shape. The dashed line box in Fig. 9a is the neutron source area, and the solid line box represents the stacked-structure area. The neutron flux density significantly declined after passing through the reflector and shield to approximately 5×10^8 n/(cm^2·s), which meets the design requirement of less than 5×10^9 n/(cm^2·s) according to the "NB/T 20194-2012 PWR Nuclear Power Plant Radiation Shielding Design Guidelines", and indicates that the shielding design of the subcritical system played a role. A more detailed neutron flux density distribution in the stacked-structure region is shown in Fig. 9b. Evidently, the neutron flux density in most areas of the stacked structure was higher than 10^{11} n/(cm^2·s). Further, the neutron flux density reached a maximum at the middle position and a minimum at the corners of the stacked structure, and the neutron flux density in the four edge corners was the smallest owing to edge effects.

Origin 0 is the geometric center of the subcritical system; the *r*-axis represents the relative radius while the *h*-axis represents the relative height.

The neutron energy spectra of the inner multiplier, inner LEU solution, and reflector are shown in Fig. 10. After passing through the LEU solution, the thermal neutron flux significantly decreased, indicating that the neutrons were effectively used. However, a high neutron flux remained in the reflector, which should be further optimized in the

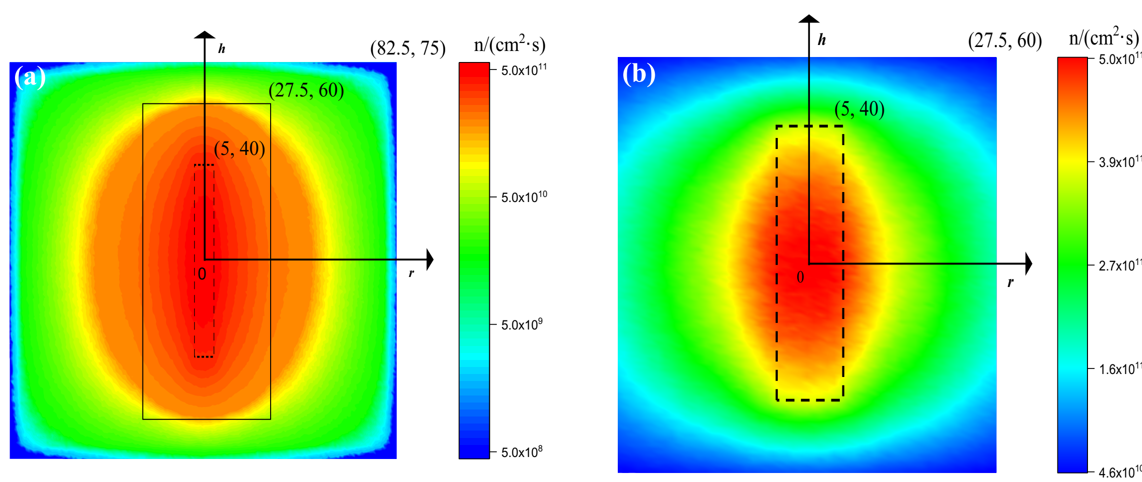

Fig. 9 (Color online) The neutron flux density distribution in **a** the subcritical system; and **b** the stacked structure

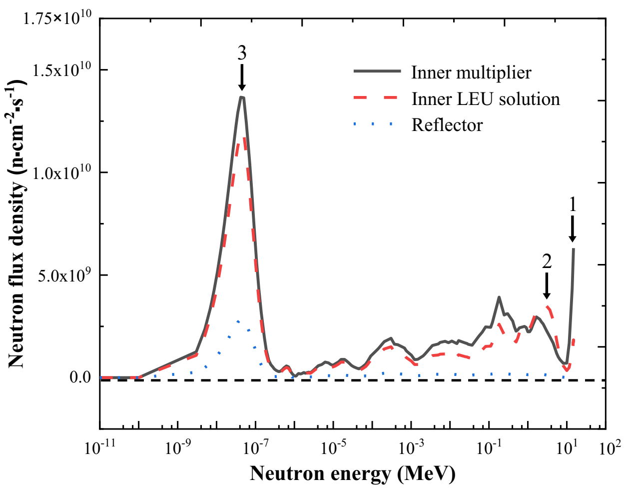

Fig. 10 Neutron energy spectrum in different functional areas of the subcritical system. The energies of peak "1," "2" and "3" are 14.1 MeV, ~ 5 MeV, and ~ 0.05 eV, respectively

future to effectively use these neutrons. Peak "1" at the neutron energy of 14.1 MeV in the inner multiplier gradually disappeared after the moderation and adsorption effect of the materials of each layer. Owing to the fission reaction of ^{235}U, an obvious peak "2" appeared in the fast neutron energy region (~ 5 MeV) in the inner LEU solution. Peak "3" is caused by the moderation of neutrons and Maxwell's equilibrium being reached in the thermal neutron zone (~ 0.05 eV); the neutron flux density decreases layer by layer due to the absorption effect. The neutron flux density in the reflector was smaller than that in other areas, indicating that the system had a better utilization of neutrons. Altogether, the excellent thermal neutron flux in the stacked structure is conducive to the production of ^{99}Mo.

3.4 Calculation of heat deposition in the subcritical system

The heat deposition in the subcritical system was calculated using an F6 tally card to roughly estimate the temperature distribution inside the LEU solution. The heat deposition appeared as obvious boundaries between the parts of the subcritical system, while the power deposition distribution in the LEU solution region was similar to that of the neutron flux density distribution, displaying an elliptical shape, as shown in Fig. 11a. Compared with other areas, the LEU solution had the largest thermal deposition owing to the heat generated by ^{235}U fission. The reaction heat was mainly deposited in the middle and inside of the inner LEU solution, and the heat deposition could reach as high as 0.1 W/cm^3 in part of the inner LEU solution. The horizontal heat distribution at $h = 0$ cm (solid line in Fig. 11a) is shown in Fig. 11b. The energy deposition in other areas, such as the multiplier, is markedly smaller than that of the LEU solution. The inner LEU solution had the largest thermal deposition, whereas the outer LEU solution had the smallest thermal deposition. This result is due to the gradual decrease in the neutron flux density from the inside to the outside. The vertical heat distribution in the middle of the uranium solution at $r = 15$ cm (i.e., the dash-dot line in Fig. 11a) is shown in Fig. 11c. The heat distribution curve was relatively smooth and almost completely symmetrical to the r-axis, indicating that the divided cells in the model are sufficiently small and the calculation error control is reasonable. The average and total heating power in the LEU solution were approximately 0.074 W/cm^3 and 14.67 kW, respectively, indicating that the fuel solution will boil within 2 h without the addition of any cooling design. Considering the cooling system, the inlet H_2O coolant velocity of 1.0 m/s and temperature of 20 °C are sufficient to ensure that the temperature of the fuel solution remains below 90 °C according to the simulation results of COMSOL. The void coefficient was − 106 ± 3 pcm, which indicates that the system will continue in a subcritical safety state if the temperature of the LEU solution increases and gas is generated.

4 Conclusion

Herein, a stacked structure developed by alternately assembling the multiplier and LEU solution was proposed to further improve the utilization of neutrons based on a previous study. SuperMC was used to explore the impact of the stacked structure on the neutronics performance of the subcritical system driven by a D-T neutron source. COMSOL was used to evaluate the performance of the cooling system. By carrying out neutronics and thermal analysis of the subcritical system, the following conclusions were drawn:

1. The subcritical system has the best neutron utilization rate with the Zr-4 alloy as the container material, H_2O as the coolant, and three as the number of stacked pairs.
2. The calculated k_s and void coefficient were 0.954 and − 106 ± 3 pcm, respectively, indicating that the system is in an intrinsic safe state.
3. The average and total heat deposition in the solution were approximately 0.074 W/cm^3 and 14.67 kW, respectively. The inlet H_2O coolant velocity of 1.0 m/s and initial temperature of 20 °C were sufficient to prevent boiling of the fuel solution.
4. The fuel burnup reached 3542 kWd/kgU after 10 years of operation, consuming 2.2% of ^{235}U and

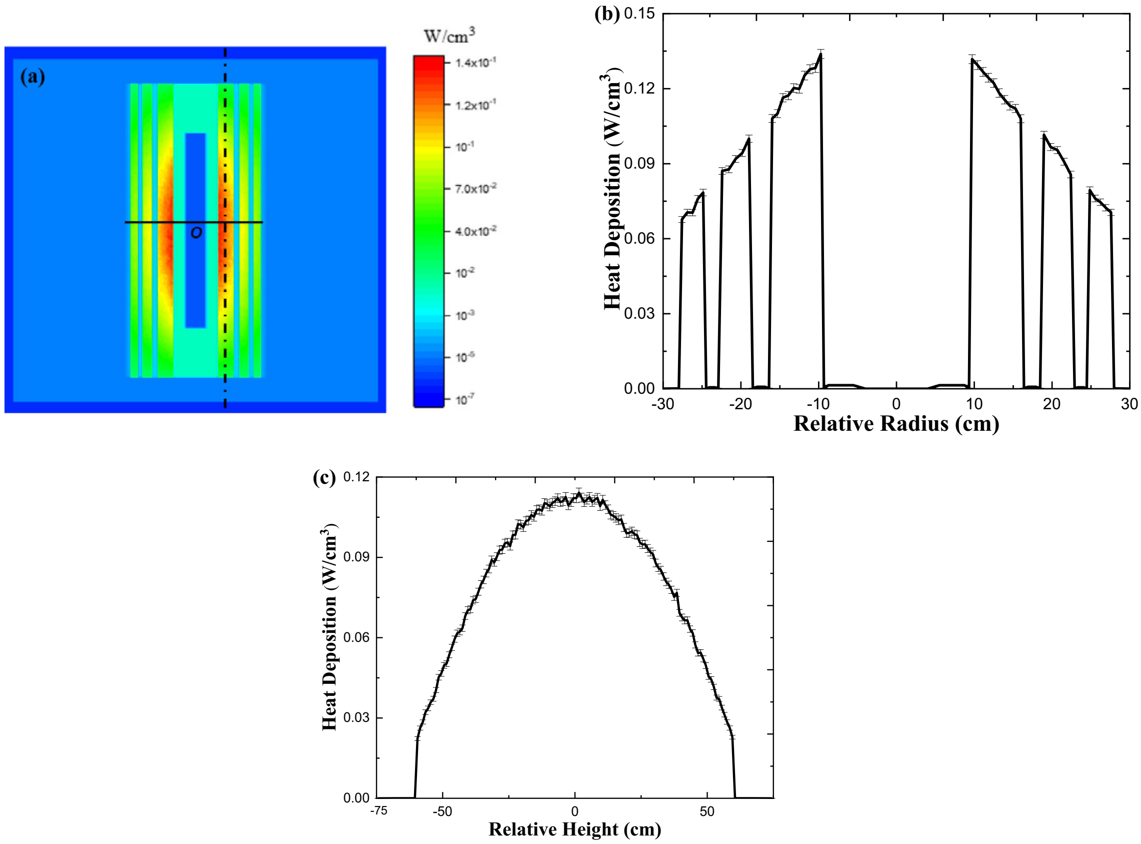

Fig. 11 (Color online) **a** Distribution of heat deposition inside the system; **b** horizontal heat distribution at h = 0 cm (on the surface of the solid line in **a**); **c** vertical heat distribution in the middle of the LEU solution at r = 15 cm (on the surface of the dashed line in **a**)

accumulating 3.788 g of ^{239}Pu. The consumption rate of the fissile material ^{235}U was found to be insignificant, and the system displayed excellent nuclear proliferation resistance.

5. The maximum yield of ^{99}Mo was 182 Ci/day, which indicates that the stacked structure can increase the ^{99}Mo yield by 16% compared to the single-layer structure.
6. The stacked structure improved the reactivity of the subcritical system by enabling full utilization of the neutrons scattered in the source direction.

This study provides a new method to improve the utilization of source neutrons in subcritical systems to produce medical radioisotopes. The results obtained herein are consistent with those of other studies in this category. However, the safety and economic feasibility of this new ^{99}Mo production method needs to be further estimated, including the analysis of thermal hydraulics, system structure, and gas generation, to ensure the safe and reliable operation of the production system.

Acknowledgments We would like to thank the students and teachers of the Institute of Nuclear Energy Safety Technology for their support and help.

Author contributions All authors contributed to the study conception and design. Material preparation, data collection and analysis were performed by Lei Ren, Yun-Cheng Han and Jia-Chen Zhang. The first draft of the manuscript was written by Lei Ren, and all authors commented on previous versions of the manuscript. All authors read and approved the final manuscript.

References

1. R. Noorden, The medical testing crisis. Nature **504**, 202–204 (2013). https://doi.org/10.1038/504202a
2. S. Qaim, S. Sudár, B. Scholten et al., Evaluation of excitation functions of ^{100}Mo (p, d+pn) ^{99}Mo and ^{100}Mo (p, 2n) ^{99m}Tc reactions: estimation of long-lived Tc-impurity and its implication on the specific activity of cyclotron-produced ^{99m}Tc. Appl. Radiat. Isotope **85**, 101–113 (2014). https://doi.org/10.1016/j.apradiso.2013.10.004
3. L. Filzen, L. Ellingson, A. Paulsen et al., Potential ways to address shortage situations of Mo-99/Tc-99m. J. Nucl. Med. Technol. **45**, 283–295 (2017). https://doi.org/10.2967/jnmt.116.185454
4. Q. Deng, M. Li, Z. Cheng, Application of ^{99}Mo production through medical isotope production reactor (MIPR). Nucl. Sci. Eng. **26**, 165–167 (2006) (in Chinese)
5. M. Pillai, A. Dash, F. Knapp, Sustained availability of ^{99m}Tc: Possible paths forward. J. Nucl. Med. **54**, 313–323 (2013). https://doi.org/10.2967/jnumed.112.110338

6. A. Youker, S. Chemerisov, M. Kalensky et al., A solution-based approach for Mo-99 production: considerations for nitrate versus sulfate media. Sci. Technol. Nucl. Install. **203**, 195–203 (2013). https://doi.org/10.1155/2013/402570
7. Z. Gholamzadeh, S. Feghhi, S. Mirvakili et al., Computational investigation of ^{99}Mo, ^{89}Sr, and ^{131}I production rates in a subcritical $UO_2(NO_3)_2$ aqueous solution reactor driven by a 30-MeV proton accelerator. Nucl. Eng. Tech. **47**, 875–883 (2015). https://doi.org/10.1016/j.net.2015.08.004
8. F. Rahmani, A. Khotbesara, F. Ghasemi, Feasibility study of Mo-99 production using high-power electron linac: nuclear and thermal-mechanical analysis based on photo neutron interaction. Radiat. Phys. Eng. **2**, 9–17 (2021). https://doi.org/10.22034/RPE.2021.252856.1026
9. S. Lee, S. Lee, M. Kang et al., Development of fission ^{99}Mo production process using HANARO. Nucl. Eng. Tech. **52**, 1517–1523 (2019). https://doi.org/10.1016/j.net.2019.12.019
10. A. Youker, S. Chemerisov, P. Tkac et al., Fission produced ^{99}Mo without a nuclear reactor. J. Nucl. Med. **58**, 514–517 (2016). https://doi.org/10.2967/jnumed.116.181040
11. Y. Nagai, Y. Hatsukawa, Production of ^{99}Mo for nuclear medicine by ^{100}Mo(n,2n) ^{99}Mo. J. Phys. Soc. Jpn. **78**(3), 201–205 (2009). https://doi.org/10.1143/jpsj.78.033201
12. O. Artun, Investigation of production of medical ^{82}Sr and ^{68}Ge for ^{82}Sr/^{82}Rb and ^{68}Ge/^{68}Ga generators via proton accelerator. Nucl. Sci. Tech. **29**, 137 (2018). https://doi.org/10.1007/s41365-018-0474-1
13. P. Tkac, D. Rotsch, M. Brown et al., Chemical processing activities for ^{99}Mo production by (γ, n) and (n, γ) reactions using enriched ^{100}Mo and ^{98}Mo targets, in *Proceedings of the 2015 ^{99}Mo Topical Meeting* (Boston, USA, 31 Aug 2015)
14. A. Qaaod, V. Ulik, ^{226}Ra irradiation to produce ^{225}Ac and ^{213}Bi in an accelerator-driven system reactor. Nucl. Sci. Tech. **31**, 44 (2020). https://doi.org/10.1007/s41365-020-00753-2
15. K. Mangera, K. Ogbomo, R. Zriba et al., Processing and evaluation of linear accelerator-produced ^{99}Mo/^{99m}Tc in Canada. J. Radioanal. Nucl. Chem. **305**, 79–85 (2015). https://doi.org/10.1007/s10967-015-3997-5
16. L. Chen, R. Yan, X. Kang et al., Study on the production characteristics of ^{131}I and ^{90}Sr isotopes in a molten salt reactor. Nucl. Sci. Tech. **32**, 33 (2021). https://doi.org/10.1007/s41365-021-00867-1
17. X. Kang, G. Zhu, R. Yan et al., Evaluation of ^{99}Mo production in a small modular thorium based molten salt reactor. Prog. Nucl. Energ. **124**, 103337 (2020). https://doi.org/10.1016/j.pnucene.2020.103337
18. D. Glenn, A. Heger, W. Hladik, Comparison of characteristics of solution and conventional reactors for ^{99}Mo production. Nucl. Technol. **118**, 142–150 (1997)
19. Z.X. Fang, M. Yu, Y.G. Huang et al., Theoretical analysis of long-lived radioactive waste in pressurized water reactor. Nucl. Sci. Tech. **32**, 72 (2021). https://doi.org/10.1007/s41365-021-00911-0
20. D. Perez, D. Lorenzo, D. Brayner et al., Neutronic evaluation of the steady-state operation of a 20 kWth aqueous homogeneous reactor for Mo-99 production. Ann. Nucl. Energ. **128**, 148–159 (2019). https://doi.org/10.1016/j.anucene.2019.01.002
21. Y. Wu, L. Chao, G. Song et al., Development of high intensity D-T fusion neutron generator (HINEG). Epj Web Conf. **153**, 03006 (2017). https://doi.org/10.1051/epjconf/201715303006
22. Z. Gholamzadeh, S. Feghhi, S. Mirvakili et al., Computational investigation of ^{99}Mo, ^{89}Sr, and ^{131}I production rates in a subcritical $UO_2(NO_3)_2$ aqueous solution reactor driven by a 30-MeV proton accelerator. Nucl. Eng. Technol. **47**, 875–883 (2015). https://doi.org/10.1016/j.net.2015.08.004
23. S. Chemerisov, A. Youker, A. Hebden et al., Development of the mini-SHINE/MIPS experiments at ANL. Trans. Am. Nucl. Soc. **107**, 74–77 (2012)
24. S. Syarip, Design and development of subcritical reactor by using aqueous fuel for Mo-99 production. Proc. Pak. Acad. Sci. **55**, 21–26 (2018)
25. L. Pardo, P. Daylen, P. Daniel et al., Coupled multi-physics simulation for the evaluation of an accelerator-driven aqueous homogeneous subcritical system for medical isotope production. Prog. Nucl. Energ. **134**, 103–117 (2021). https://doi.org/10.1016/j.pnucene.2021.103692
26. L. Ren, Z. Li, Y. Han et al., Neutronics study of a subcritical system driven by external neutron source for ^{99}Mo production. Fusion Eng. Des. **165**, 112–125 (2021). https://doi.org/10.1016/j.fusengdes.2021.112263
27. Y. Wu, C. Liu, G. Song et al., Design and research of HINEG for high current deuterium-tritium fusion neutron source. Nucl. Sci. Eng. **36**, 77–83 (2016) (in Chinese)
28. L. Seenappa, H. Manjunatha, K. Sridhar et al., Gamma and X-ray radiation compatibility of Ti–Ta–Hf–Zr alloys used for coronary stent applications. Nucl. Sci. Tech. **29**, 3 (2018). https://doi.org/10.1007/s41365-017-0339-z
29. M. Chadwick, M. Herman, P. Oblozinsky et al., ENDF/B-VII.1 nuclear data for science and technology: cross sections, covariances, fission product yields and decay data. Nucl. Data Sheets **112**, 2887–2996 (2011). https://doi.org/10.1016/j.nds.2011.11.002
30. Q. Zhu, Y. Shi, D. Hu, Research on source multiplication method in nuclear criticality safety. Atomic Energy Sci. Technol. **39**, 97–97 (2005) (in Chinese)
31. Y. Wu, J. Zhou, L. Hao et al., Research and development of hybrid evaluation nuclear database system HENDL3.0 and its application in advanced nuclear energy system design. **02**, 76–83 (2017) **(in Chinese)**
32. L. Qiu, *Introduction to Nuclear Energy Physics and Technology* (University of Science and Technology of China Press, 2012)
33. G. Sun, M. Cheng, Development of a MCNP5 and ORIGEN2 based burnup code for molten salt reactor. Nucl. Sci. Tech. **27**, 65 (2016). https://doi.org/10.1007/s41365-016-0070-1